IOP Conf. Series: Materials Science and Engineering **375** (2018) 012016 doi:10.1088/1757-899X/375/1/012016

Segregation affecting the evolution of primary recrystallization textures in a ternary Fe-Si-Sn alloy

N Mavrikakis[1,2,*], P R Calvillo[3], W Saikaly[3], M Descoins[1], D Mangelinck[1] and M Dumont[1]

[1] Aix Marseille Université, CNRS, IM2NP UMR 7334, 13397, Marseille, France
[2] ArcelorMittal Maizières Research SA, Voie Romaine, BP 30320, 57283, Maizières les Metz, France
[3] ArcelorMittal Global R&D, Technologiepark 935, BE-9052, Zwijnaarde, Belgium
[*]email address: nikolas.mavrikakis@im2np.fr

Abstract

The effect of Sn addition on the primary recrystallization of cold rolled Fe-3 wt. % Si alloys is investigated. Texture evolution and misorientation distributions are analyzed on partially recrystallized samples using the electron backscatter diffraction technique (EBSD). Sn was found to affect the microstructure, throughout the thermal treatment of the materials, by refining the grains and altering the texture. In the presence of Sn, the intensity of {111}<*uvw*> grains is reduced through all stages of recrystallization, while that of {100}<*uvw*> and {*hkl*}<100> grains is increased. The favored growth of these latter grains is most likely due to a combination of mechanisms that involve nucleation site preferences and probably the presence of high mobility CSL boundaries. Σ5 boundaries were observed to increase in frequency with Sn through all stages of recrystallization. Additionally {100} grains were found to be most frequently correlated with Σ5 interfaces, which might be due to geometrical considerations. Site-specific characterization of grain boundaries was conducted with three-dimensional atom probe tomography (3D-APT) to measure the grain boundary segregation of Sn.

1. Introduction

The Fe-Si system is well known for studying annealing phenomena, as it is single-phase ferritic for Si content above 1.9 wt. % [1]. The overall recrystallization process, during annealing of the as cold rolled sheet, is characterized by a strong γ-fiber texture with the peak of intensity depending on the rolling reduction [2,3]. Nevertheless, adding trace elements such as P, Sb and Sn has a great impact on the texture development thanks to the promotion of selective grain growth, due to surface and grain boundary segregation phenomena [4].

More specifically, Sn segregation has been found to strongly affect the recrystallization texture of iron, by selectively promoting the grain growth of grains with specific texture. {111}<uvw> texture components were often weakened whilst the growth of {110} grains was mainly favored [4–6]. In some other studies, Sn favored the {100}<uvw>, {hkl}<100> oriented grains, in most cases strengthening the Goss component [7]. Nakashima et. al observed that Sn facilitates secondary recrystallization and increases the migration rate of special (CSL) boundaries, like Σ9 [7]. In the literature, special properties are often attributed to CSL boundaries such as low energy and high mobility. The low energy aspect of CSL boundaries is believed to be the most important by Hutchinson and Hasson [8,9], while Lücke and others highlight the enhanced mobility of low Σ boundaries, as the most important aspect of these interfaces [10]. Harase [11] reports that CSL boundaries become more mobile in the presence of solutes or precipitates, as the latter inhibit less

mobile grain boundaries from growing. He also suggests that Σ5 boundaries become more mobile than Σ9 boundaries at lower temperatures.

Literature on Sn interaction with the microstructure during annealing is scarce, mainly the effect of Sn after the recrystallization and grain growth are completed, is addressed. Such studies are mainly focused on the contribution of Sn on secondary recrystallization, which assists the Goss texture formation. While, the interfacial segregation of Sn was usually analyzed with Auger Electron Spectroscopy (AES), in randomly opened grain boundaries, after brittle intergranular fracture [12]. Therefore, the present study evaluates the texture evolution during the phenomenon of recrystallization, from the nucleation stages and through the growth of the recrystallized grains, considering the effect of Sn grain boundary segregation and its potential impact on the as developed crystallographic texture. For the means of this research, the site-specific technique that combines EBSD, focused ion beam (FIB) and 3D-APT, will be employed to analyze the grain boundary segregation of Sn, at the near-atomic scale and in combination with orientation data.

2. Experimental

A binary Fe – 3Si and a ternary Fe – 3Si – 0.1Sn (wt. %) were laboratory vacuum cast with maximum impurity level of 200 ppm. The binary alloy provided a reference material to isolate the silicon contribution and be able to characterize the Sn effect in the microstructure evolution of iron. Both materials were similarly processed, with a final cold rolling step at a Von Mises true strain of about $\varepsilon = 2$.

Subsequently, the as cold rolled materials were heat treated using a BAHR dilatometer, at a constant heating rate, following interrupted annealing schemes to monitor the primary recrystallization kinetics at 700°C. After the isothermal soaking, samples were quenched to room temperature to ensure that no segregation occurs during cooling and in order to freeze the microstructure. Following the processing, materials were metallography prepared and optically examined in a Keyence VHX-5000 digital microscope. The recrystallization volume fractions were first quantified using the point counting method, considering from 400 to 500 points [13]. Samples at fraction of volume recrystallized, X_v = 0.2, 0.5 and 0.8 were selected to be further analyzed in EBSD.

The EBSD scans were acquired covering a minimal area of 900 x 300 μm^2 with a step size of 0.5μm. The number of recrystallized grains included in the mappings, and consequent analysis, range from 2400 to 4000 grains, which are statistically sufficient to derive reliable conclusions. Recrystallized (RX) grains were defined as new, almost dislocation free grains, bounded by high-angle grain boundaries (HAGBs), $\theta \geq 15^o$, with a grain internal misorientation not exceeding 2^o. The grain shape should be close to equiaxed, having a maximum aspect ratio of 3:1. The post-processing was performed in both HKL Channel 5 and OIM Analysis platforms. From the EBSD scanned areas, grain boundaries of the recrystallization front, migrating boundaries between RX and the surrounding not-recrystallized (not-RX) structure, were selected and prepared for 3D-APT, in a FEI Helios NanoLab 600 FIB, following the lift-out technique [14]. Atom probe experiments were conducted in a Cameca LEAP 3000XHR instrument, with a detector efficiency of 37%. Measurements were performed in voltage mode, while the sample temperature and fraction of electric pulses were selected at 70K and 20% respectively. 3D-APT data were reconstructed after proper calibration of the reconstruction parameters, as described by Gault et. al [14]. Finally, the quantification of segregation has been performed with the, well-established, Gibbsian excess method [15].

3. Results

3.1. Recrystallization kinetics

Before analyzing the kinetics, the conversion from non-isothermal (during continuous heating) to isothermal time was made, according to the Whittaker and Sellars approach [16]. The Johnson-Mehl-Avrami-Kolgomorov (JMAK) equation was used to characterize the recrystallization kinetics:

$$f_{REX} = 1 - exp(-Kt^n) \quad (1)$$

where f_{REX} is the recrystallized volume fraction at a given time, *t*, *n* is the Avrami exponent and *K* is a kinetic coefficient. The JMAK description of isothermal kinetics was fitted, using the least-squares analysis, to obtain a best-fit for the Avrami plot, ln(ln(1/(1-X))) vs. ln(t) plot. The Avrami exponent, *n*, was found experimentally to be $n \approx 1$ for both alloys, and according to Christian [17] the recrystallization is then a phenomenon of interface controlled growth in a condition of grain boundary nucleation with site saturation. Sn addition was found to retard the recrystallization kinetics, figure 1(a).

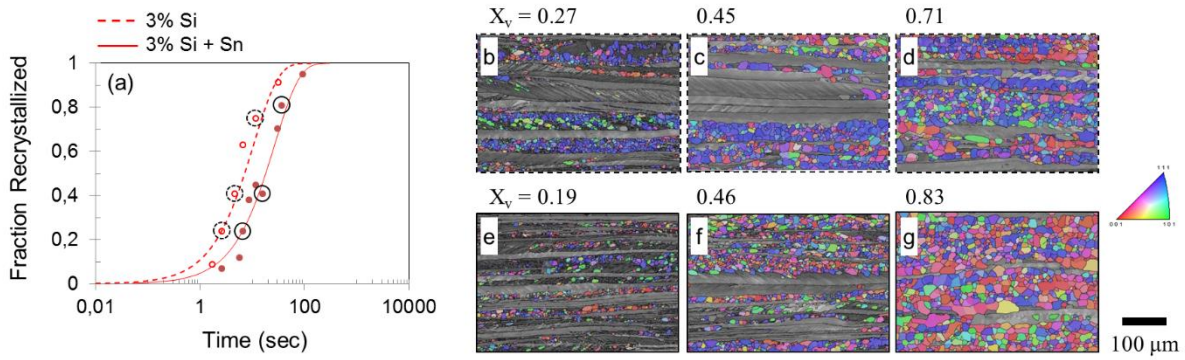

Figure 1. (a) Recrystallization kinetics of the materials, quantitative metallography data fitted with the JMAK equation. (b-d) Partial recrystallization EBSD ND-IPF mappings for the binary alloy and (e-g) for the ternary alloy. The recrystallization volume fractions measured by EBSD are shown for comparison and marked with circles on the kinetics plot.

The EBSD ND-IPF maps are illustrated for the two materials in figure 1(b-g), where all restored grains (recovery and recrystallization products) are highlighted, while the not recrystallized structure is shown in grey scale. The recrystallized volume fractions as determined by the EBSD were in very good agreement with the quantitative metallography values and are indicated in figure 1 as black circles. It is observed that large colonies of primary recrystallized grains are present within certain deformation bands while other regions remain in an entirely deformed state. Such behavior is well known in many cases of recrystallization in ultra-low carbon and other bcc steels and is considered to arise due to the variation in stored energy between grains of different orientations in the deformed structure [18,19].

3.2. Recrystallization textures

Analyzing the recrystallized texture from the EBSD, figure 2; the binary alloy, figure 2(a-c), is found to have strong recrystallization texture [3]. From the early stages of recrystallization, the binary alloy texture, has a strong {111}<112> component that remains during growth. The texture does not change significantly as recrystallization advances. On the other hand, in the ternary alloy, figure 2(d-f), the texture of recrystallized grains is significantly weaker. At the early stages, intensities of the γ-fiber are dispersed quite evenly, with the {111}<112> component clearly weaker compared to the

binary. At the same time, the strongest texture component is the Goss {110}<100>. As recrystallization progresses, the more random character of texture is maintained, the γ-fiber is weakened at the {111}<110> component while the Goss is still present.

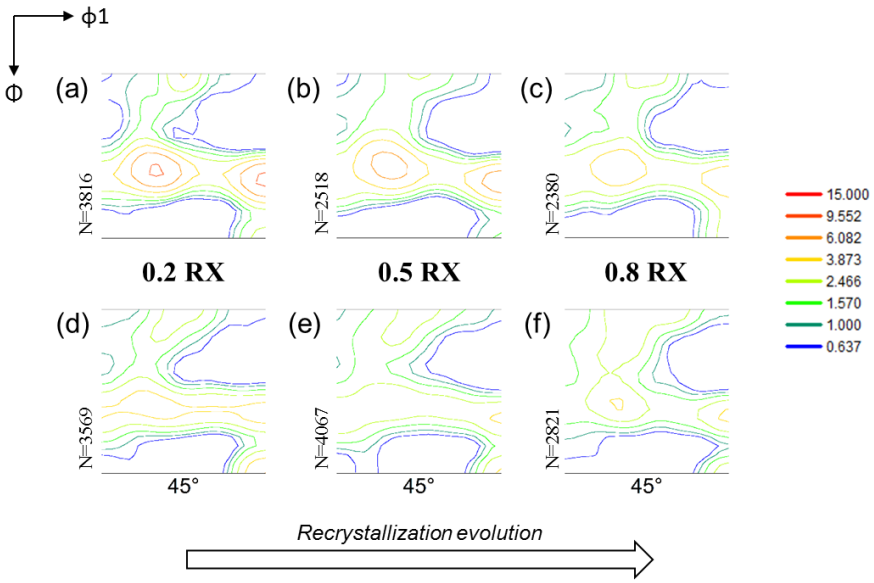

Figure 2. Micro-texture ODFs at the φ_2=45° section of the Euler space of all restored grains during the progress of recrystallization. (a-c) The texture of the binary and (d-f) the ternary alloy, along with the number of grains that were included in the analysis.

Figure 3 shows the texture densities along the main fibers, η, α and γ-fibers, and can provide a more quantitative insight on the stages intensities of the various texture components. It can be seen that the effect of Sn is stronger at the early of recrystallization, where the Goss component with Sn is at about x6 random intensity, compared to about x2 in the case of the binary alloy. Also, the most pronounced decrease of the {111}<112> component is found at this stage; the ternary alloy was found to have a x4 random intensity compared to the binary which has a relative intensity of about x14 random.

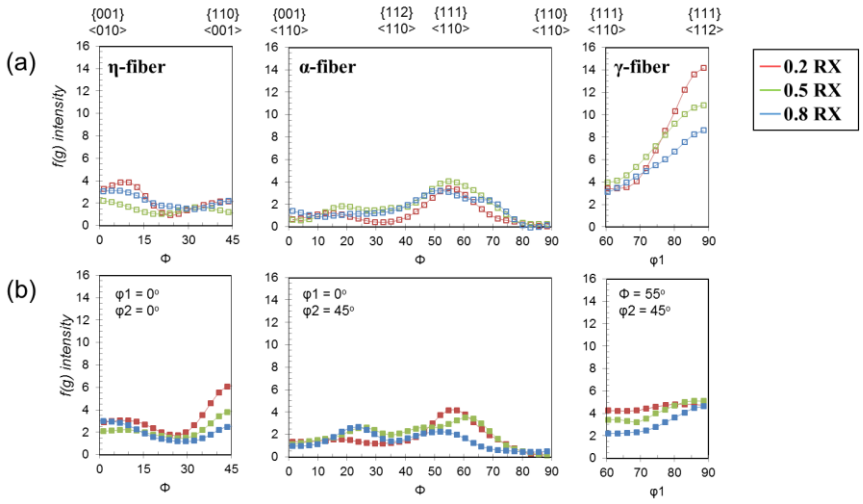

Figure 3. Texture densities along the main fibers observed in bcc steels (η, α, γ-fibers) for the binary (a) and the ternary (b) alloys.

As recrystallization advances these differences in texture remain, however weaken. It is thus believed that Sn addition might have a stronger effect during the nucleation stage of recrystallization.

3.3. CSL boundary distribution

Analyzing the frequency of CSL boundaries of the entire scanned areas, it is seen in figure 4(a) that the CSL fraction is increasing with the progress of recrystallization in both binary and ternary alloy. Σ3 boundaries were not displayed here as there is no twinning observed in these alloys, and Σ3 are generally known to be less mobile. The Σ3 boundaries in this case represent a 60° <111> rotation that is frequently found between two γ-fiber grains and between the {111}<112> and the {001}<110> texture components.

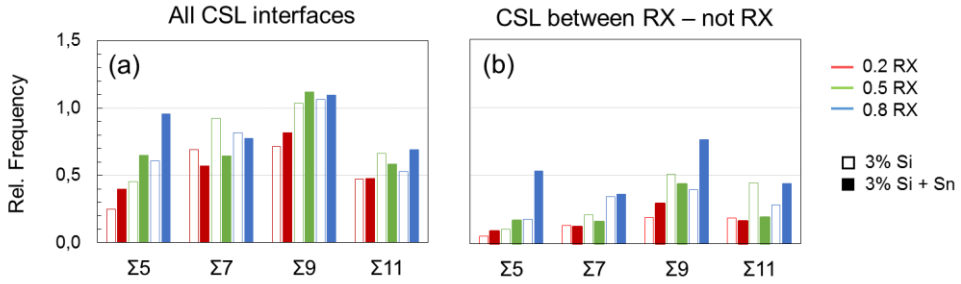

Figure 4. The relative frequencies of low Σ, CSL boundaries as measured in the binary (empty bars) and the ternary (solid bars) alloys, shown as a function of recrystallized fraction (increasing fraction from left to right). (a) is the CSL boundary distributions in the entire scan, (b) is the CSL distributions only between RX and not RX grains (for interpretation of the references to color in this figure, the reader is referred to the web version of this article).

To better quantify the CSL fraction, an analysis was made within the data to evaluate the CSL between RX grains and between RX and not-RX grains. The former classification illustrated a change in CSL fraction as RX grains grow during recrystallization however, it was not very different between the binary and ternary alloy. On the contrary, by analyzing the relative frequency of CSL boundaries of the recrystallization front, figure 4(b), it can be seen that as recrystallization progresses, and especially at 0.8 RX, the total fraction of CSL boundaries is increased with Sn. In particular, it is observed that Σ5 36.87° <100> boundaries have a steady increase in the ternary alloy. A systematic evaluation of the CSL fraction at various temperatures and stages of restoration between the two alloys (unpublished work), showed that the ternary alloy has a consistently higher fraction of Σ5 boundaries.

4. Discussion

Textures were measured in a binary (Fe-Si) and a ternary (Fe-Si-Sn) alloy, to evaluate the effect of Sn on texture evolution during static recrystallization. On one hand, the binary alloy illustrated typical recrystallization textures of low carbon steels [3], with strong rolling texture due to prior cold rolling. On the other hand, the texture of the ternary alloy was found to have less features of the rolling texture, the γ-fiber was remarkably reduced in the recrystallized texture, and at the same time, the peak of intensity was at the Goss component. Previous authors have reported such behavior with the addition of Sn in the fully annealed texture, and also when alloying with other surface active elements as P or Sb [5–7].

The texture observations suggest that Sn has a more profound effect during the early stages of recrystallization. In rolled bcc steels, the sub-grain growth process often takes place preferentially in the vicinity of prior grain boundaries and at the shear bands of {111} deformed grains [19]. It may

be suggested that Sn segregation at prior grain boundaries may decrease the probability of recrystallization nucleation from the prior boundaries. Prior grain boundaries, are known to be the main nucleation site of γ-fiber grains [18], while at shear bands of {111}<112> grains, nucleation of mainly Goss {110}<001> grains is taking place [20]. This possible effect of Sn on nucleation of recrystallization has been previously mentioned in literature [5].

Moreover, Sn segregation on the recrystallization front might have an added effect on the recrystallized microstructure, through affecting the grain boundary mobility. Special grain boundaries are considered to have higher mobility than general ones [21]. Aust and Rutter [22] have studied grain boundary migration velocity under the effect of Sn in pure Pb. For general and special (CSL) HAGBs, they observed that Sn, even at trace levels (a few ppms), decreases the boundary migration velocity considerably. The effect is more remarkable in the case of general grain boundaries. In the CSL boundaries, although there is an observed solute drag, the effect is weaker.

The segregation of Sn was quantified with 3D-APT in a site-specific manner. The grain boundary character is taken into account before the region of interest is selected. Initially, general HAGBs of the recrystallization front (schematic shown in figure 5a), were preferred for analysis, as these boundaries represent the majority of the migrating interfaces. Figure 5(c) shows a typical volume from 3D-APT, view from two different perspectives, for the Sn atoms and their enrichment at a general HAGB. Results show that Sn segregates at general HAGBs, at concentrations between 1-1.4 at. % (0.4-0.6 at. nm^{-2} excess number of atoms).

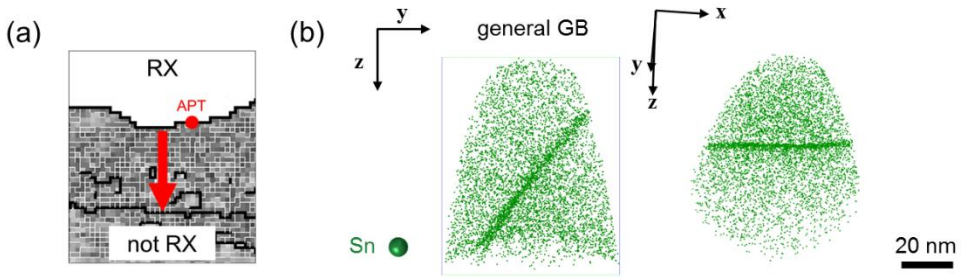

Figure 5. (a) Schematic of the recrystallization front where segregation analysis was made with 3D-APT and (b) a 3D volume for Sn atoms showing segregation at a general GB.

In this study, the segregation of Sn at general HAGBs was measured and assuming that Sn decreased the migration velocity of grain boundaries in bcc α-Fe in a similar trend as Aust and Rutter observed, it is suspected that its segregation at general grain boundaries will increase the contrast in grain boundary mobility between general and CSL boundaries. Therefore, orientations associated with high mobility CSL boundaries might exhibit a preferential growth, which might be the case of the Σ5 36.87° <100> that were found to consistently increase with Sn.

In general, it was observed that in the ternary alloy there is a significant increase in all CSL boundaries at the recrystallization front (figure 4b). In order to evaluate the potential contribution of CSL on the texture development, the case of Σ5 was explored. The deformed state texture was taken as the matrix texture, figure 6(a), and the product orientations were calculated applying a Σ5 36.87° <100> rotation to the main bcc texture components, present in the matrix texture. Figure 6(b) shows the product orientations superimposed on the recrystallization (0.8) texture of the ternary alloy. Careful examination of this figure shows that some of these components are found to be Σ5 related orientations that are present in the texture after recrystallization, however, the recrystallization texture cannot be explained only by the Σ5. Additionally, it can be observed that most of these Σ5 rotations, result along the {100}<uvw> (θ-fiber) and the {hkl}<100> (η-fiber) orientations, figure 6(c). Thus, it is observed that Σ5 have an orientation relationship with {100}<uvw> and {hkl}<100>

grains, as statistically have a higher possibility to bound these fibers due to their common <100> axis of rotation.

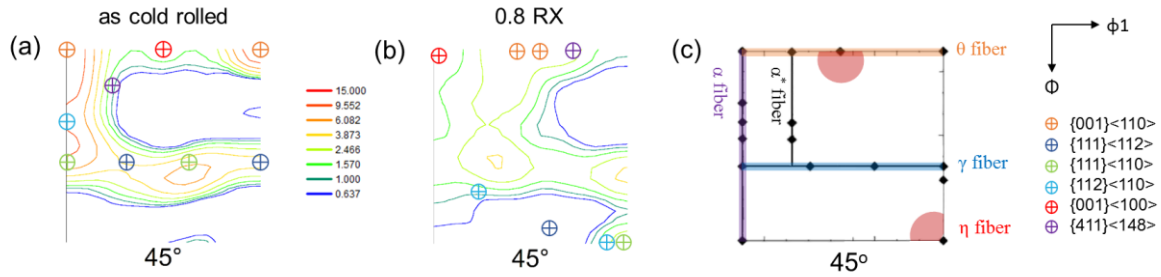

Figure 6. The calculated peak positions for Σ5 relationships, from the matrix (a) as cold rolled to the recrystallization texture (b) in the ternary alloy, recrystallization texture at $X_v=0.8$. The symbols indicate the calculated Σ5 rotations from the deformed to the recrystallization texture for main texture components often observed in bcc steels and (c) is an illustration of the main texture fibers.

Further investigation needs to be made on the potential Σ5 role during recrystallization, and whether their orientation relationship with {100} grains can give to these latter grains, the sufficient size advantage to survive the grain growth process. This could occur as Sn is prone to segregate in HAGBs and will therefore decrease their migration rate, as Aust and Rutter observed. Additional grain boundary segregation analyses is needed to be performed along with an evaluation of the potential solute drag effect of Sn on migrating grain boundaries.

5. Conclusions

Research study on Fe – 3Si binary and Fe – 3Si – 0.1Sn (wt. %) ternary alloy was conducted to evaluate the texture evolution in the presence of Sn, during static recrystallization after cold deformation. It was observed that Sn addition resulted in a recrystallization texture with weaker rolling components. {111}<112> component was decreased meanwhile a clear promotion of Goss texture component was suggested. Sn segregation could affect recrystallization texture at two stages of the process:

- at the stage of nucleation

By modifying the nucleation site preferences. If Sn segregates to prior grain boundaries it would reduce the grain boundary energy, thus it could decrease the nucleation of recrystallized grains from such sites. As an aftermath, nucleation of γ-fiber grains which tend to nucleate at prior grain boundaries will be reduced. In the meantime, nucleation at the shear bands is not affected, Goss component, which nucleates preferably at shear bands, will be favored with Sn addition.

- at the recrystallization front

By modifying the boundary migration preferences. Σ5 boundaries might be assisting the texture development of {100} grains, as there is an orientation relationship of these grains with the Σ5. Such boundaries are known to have higher mobility than general ones. These boundaries were found to have consistently higher relative frequency with Sn, at all stages of primary recrystallization but also during early stages of subsequent grain growth. More work is needed however, to validate such a hypothesis.

Acknowledgements

This project (ANRT – Project nº 1073-2015) was possible with the support of National Association of Research and Technology.

References

[1] Kubaschewski O 1982 *Iron-Binary phase diagrams*

[2] L. Kestens J J J 2005 Transformation And Recrystallization Textures Associated With Steel Processing *ASM International Volume 14A* vol 14A (ASM International) pp 685–700

[3] Raabe D and Lücke K 1992 Annealing textures of BCC metals *Scr. Metall. Mater.* **27** 1533–8

[4] Suzuki S, Kuroki K, Kobayashi H and Takahashi N 1992 Sn Segregation at Grain Boundary and Interface between MnS and Matrix in Fe-3 mass%Si Alloys Doped with Tin *Mater. Trans. JIM* **33** 1068–76

[5] Kubota T. K K Matsuo Y .Takahashi N 1996 Effect of Sn on Primary Recrystallization Texture of Fe-Si Alloy *Mater. Sci. Forum*

[6] Godec M, Jenko M, Grabke H J and Mast R 1999 Sn Segregation and Its Influence on Electrical Steel Texture Development *ISIJ Int.* **39** 742–6

[7] S. Nakashima K T JHarase, TKamijo 1996 Effect of Tin Addition on Primary and Secondary Recrystallizations of Silicon Steel *Mater. Trans.*

[8] Homma H and Hutchinson B 2003 Orientation dependence of secondary recrystallisation in silicon–iron *Acta Mater.* **51** 3795–805

[9] Hasson G C and Goux C 1971 Interfacial energies of tilt boundaries in aluminium. Experimental and theoretical determination *Scr. Metall.* **5** 889–894

[10] Shimizu R 1989 Coincidence grain boundary and texture evolution in Fe-3%Si *Acta Metall.* **37** 1241–9

[11] Harase J 1995 Coincidence boundary and secondary recrystallization in fcc and bcc metals *Can. Metall. Q.* **34** 185–93

[12] Seah M P and Hondros E D 1973 Grain Boundary Segregation *Proc. R. Soc. Math. Phys. Eng. Sci.* **335** 191–212

[13] Rossi P O and Sellars C M 1997 Quantitative metallography of recrystallization *Acta Mater.* **45** 137–148

[14] Gault B, Moody M P, Cairney J M and Ringer S P 2012 *Atom Probe Microscopy* vol 160 (New York, NY: Springer New York)

[15] Krakauer B W and Seidman D N 11 Subnanometer scale study of segregation at grain boundaries in an Fe(Si) alloy *Acta Mater.* **46** 6145–61

[16] Sellars C M and Whiteman J A 1978 Recrystallization And Grain Growth In Hot Rolling **13** 187–94

[17] Christian J W 1965 *The Theory of Transformations in Metals and Alloys* (Pergamon)

[18] Hutchinson W B 1984 Development and control of annealing textures in low-carbon steels *Int. Met. Rev.* **29** 25–42

[19] Dillamore I L, Smith C J E and Watson T W 1967 Oriented Nucleation in the Formation of Annealing Textures in Iron *Met. Sci. J.* **1** 49–54

[20] Ushioda K and Hutchinson W B 1989 Role of shear bands in annealing texture formation in 3%Si-Fe(111)[112] single crystals. *ISIJ Int.* **29** 862–7

[21] Lejcek P 2010 *Grain Boundary Segregation in Metals* (Elsevier)

[22] Aust K T and Rutter J W Grain Boundary Migration in High Purity Lead and Dilute Lead-Tin Alloys *Trans. Met. Soc. AIME* **215** 119–27